Title
Divergent responses of Atlantic coastal and oceanic Synechococcus to iron limitation

Journal
Proceedings of the National Academy of Sciences of the United States of America, 112(32)

ISSN
0027-8424

Authors
Mackey, Katherine RM
Post, Anton F
McIlvin, Matthew R
et al.

Publication Date
2015-08-11

DOI
10.1073/pnas.1509448112

Divergent responses of Atlantic coastal and oceanic *Synechococcus* to iron limitation

Katherine R. M. Mackey[a,b,1,2], Anton F. Post[b], Matthew R. McIlvin[a], Gregory A. Cutter[c], Seth G. John[d], and Mak A. Saito[a,2]

[a]Marine Chemistry and Geochemistry, Woods Hole Oceanographic Institution, Woods Hole, MA 02536; [b]Bay Paul Center for Comparative Molecular Biology and Evolution, Marine Biological Laboratory, Woods Hole, MA 02543; [c]Department of Ocean, Earth, and Atmospheric Sciences, Old Dominion University, Norfolk, VA 23529; and [d]Department of Earth Sciences, University of Southern California, Los Angeles, CA 90089

Edited by Robert Haselkorn, University of Chicago, Chicago, IL, and approved June 26, 2015 (received for review May 13, 2015)

Marine *Synechococcus* are some of the most diverse and ubiquitous phytoplankton, and iron (Fe) is an essential micronutrient that limits productivity in many parts of the ocean. To investigate how coastal and oceanic Atlantic *Synechococcus* strains acclimate to Fe availability, we compared the growth, photophysiology, and quantitative proteomics of two *Synechococcus* strains from different Fe regimes. *Synechococcus* strain WH8102, from a region in the southern Sargasso Sea that receives substantial dust deposition, showed impaired growth and photophysiology as Fe declined, yet used few acclimation responses. Coastal WH8020, from the dynamic, seasonally variable New England shelf, displayed a multitiered, hierarchical cascade of acclimation responses with different Fe thresholds. The multitiered response included changes in Fe acquisition, storage, and photosynthetic proteins, substitution of flavodoxin for ferredoxin, and modified photophysiology, all while maintaining remarkably stable growth rates over a range of Fe concentrations. Modulation of two distinct ferric uptake regulator (Fur) proteins that coincided with the multitiered proteome response was found, implying the coastal strain has different regulatory threshold responses to low Fe availability. Low nitrogen (N) and phosphorus (P) availability in the open ocean may favor the loss of Fe response genes when Fe availability is consistent over time, whereas these genes are retained in dynamic environments where Fe availability fluctuates and N and P are more abundant.

iron adaptation | *Synechococcus* | photosynthesis | quantitive proteomics | nutrient limitation

The marine *Synechococcus* are a cosmopolitan group of cyanobacteria that contribute ∼17% of marine net primary production worldwide (1) and whose diversity is linked to nutrient availability in both coastal and open ocean waters (2). Of the nutrients required by phytoplankton, the micronutrient iron (Fe) limits productivity in ∼30% of the world's oceans (3) and shapes *Synechococcus* genome content (4, 5). Seawater Fe concentrations in the euphotic zone can vary due to inputs from atmospheric, coastal, and upwelled sources. The open ocean, being more removed from these sources, is typically depleted in Fe relative to coastal waters. Consistent with these distributions, experiments on oceanic phytoplankton have found them able to grow at lower metal conditions than related coastal strains, implying a general phenomenon of open ocean phytoplankton being better adapted to low metal availability (6, 7).

The North Atlantic Ocean presents an extreme endmember with which to examine the coastal–open ocean phytoplankton adaptation phenomenon due to its large Fe flux associated with seasonal atmospheric dust deposition from the Saharan desert (8, 9). Moreover, there has been increasing evidence that Fe availability may be dynamic in coastal regions, with observations of Fe limitation of phytoplankton in eastern boundary upwelling regions upon upwelling of macronutrient-rich and Fe-depleted waters (10, 11). Whereas the diversity and distribution of *Synechococcus* strains have been linked to macronutrient availability (2), the considerable range of Fe levels across which *Synechococcus* thrive suggests they may also possess unique and diverse regulatory mechanisms for Fe acclimation.

To explore this acclimation potential in the North Atlantic context, we compared the responses of coastal and oceanic Atlantic *Synechococcus* to Fe limitation. Comparison of strain origins with trace metal and low-level nutrient measurements from the recent US North Atlantic Zonal Transect GEOTRACES expedition demonstrates large differences in nitrate, phosphate, and dissolved Fe between sites in the North Atlantic basin. The coastal strain, WH8020, was isolated from the New England shelf (Fig. 1 *A* and *B*), a region with a dynamic nutrient (12) and Fe (13) regime. Oceanic strain WH8102 was isolated from the permanently stratified southern Sargasso Sea, an oligotrophic site that consistently receives Fe from aeolian dust year round, with very high levels in the summer (8). The consistent dust supply results in higher dissolved Fe levels in the open ocean (∼0.8 nM within the Sahara dust plume) relative to North American coastal waters (Fig. 1*B*).

To test their abilities to acclimate, both strains were rendered Fe limited by sequential transfer into no-Fe-added media and were rescued with varying concentrations of Fe′ (Fe′ defined as the sum of inorganic species). Cellular protein was harvested during log-phase growth to characterize Fe responses (Fig. 2 *C* and *H*). Protein abundance was measured following cell pellet extractions of single cultures grown at each prescribed Fe concentration, followed by high-resolution LC-MS proteomic analysis for relative abundance and targeted proteomics for absolute abundance (*Materials and Methods*).

Significance

Conventional knowledge suggests that coastal phytoplankton are less able to adapt to Fe limitation than open ocean species. Here we show that in contrast to the established paradigm, coastal *Synechococcus* from the New England shelf is capable of dynamic, multitiered Fe adaptation that allows it to thrive over a broad range of Fe concentrations by partitioning Fe among different uptake and storage proteins. This protein-based response is beneficial in high nitrogen (N) waters with low and variable Fe:N ratios. An oceanic Atlantic *Synechococcus* isolate lacks this adaptive response, suggesting the small yet significant N cost of retaining Fe response proteins offsets the benefit of Fe adaptability in the southern Sargasso Sea, where N is chronically scarce and Fe:N ratios are high.

Author contributions: K.R.M.M., A.F.P., and M.A.S. designed research; K.R.M.M. and M.R.M. performed research; K.R.M.M. analyzed data; A.F.P., G.A.C., and S.G.J. contributed new reagents/analytic tools; and K.R.M.M. and M.A.S. wrote the paper.

The authors declare no conflict of interest.

This article is a PNAS Direct Submission.

Freely available online through the PNAS open access option.

Data deposition: The WH8020 genome reported in this paper has been deposited in the GenBank BioProject database (accession no. PRJNA278997).

[1]Present address: Department of Earth System Science, University of California, Irvine, CA 92697.

[2]To whom correspondence may be addressed. Email: kmackey@uci.edu or msaito@whoi.edu.

This article contains supporting information online at www.pnas.org/lookup/suppl/doi:10.1073/pnas.1509448112/-/DCSupplemental.

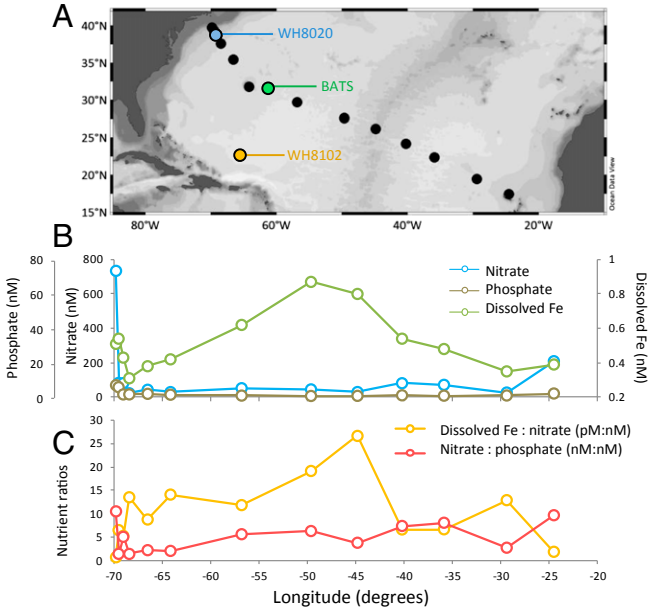

Fig. 1. (*A*) Map of the US North Atlantic Zonal GEOTRACES sampling stations and locations where *Synechococcus* WH8102 and WH8020 were isolated and the location of BATS. (*B*) Concentrations of nitrate, phosphate, and dissolved Fe along the transect from 28- to 51-m depth. (*C*) Ratios of dissolved Fe:nitrate (pM:nM) and nitrate:phosphate (nM:nM) along the transect.

We observed that the growth rate and photophysiology (F_v/F_M) of oceanic *Synechococcus* WH8102 was proportional to Fe′ concentration (Fig. 2 *A*–*D*). In contrast, coastal *Synechococcus* WH8020 tailored its response to Fe limitation through the differential expression of Fe response proteins in a multitiered, hierarchical cascade by which cells partitioned and conserved Fe, and so thrived over a broad range of Fe concentrations. Fe′ levels had a minimal effect on growth rate (Fig. 2*F*), although a sharp decline in photosynthetic protein abundance was observed below 1 nM (Fig. 2*J*), followed by a decline in photosynthetic efficiency below 0.3 nM (Fig. 2*I*). Thresholds for photosynthetic efficiency and photosynthetic protein abundance were similar between strains (Fig. 2 *D*, *E*, *I*, and *J*).

The global proteome of coastal *Synechococcus* WH8020 revealed large changes in the abundance of Fe sensing, acquisition, and storage proteins (Fig. 3*A*). Fe′ levels ≤1 nM led to induction of the Fe transport protein, IdiA, that assists in Fe uptake during periods of low Fe availability (14) and substitution of Fe-free flavodoxin for Fe-requiring ferredoxin (15, 16). At Fe′ levels above 1 nM, coastal WH8020 produced ferritin, which stores Fe when it is abundant for later use when levels decline. Several additional Fe response systems were present in WH8020 that are also shared in the genome of coastal strain CC9311 isolated from the California Coastal Current, although the latter has additional genes including a ferrous Fe uptake transporter (*feo*) (Fig. 3*B* and *SI Appendix*, Table S1). The strong proteome response of coastal WH8020 to low Fe implies that coastal Atlantic waters may share aspects of the "patchwork mosaic" dynamics of Fe limitation and excess similar to California coastal waters (10, 11).

The multitiered response in coastal WH8020 appears to be regulated by two isoforms of the ferric uptake regulator protein (Fur), which acts as a transcriptional repressor when it binds intracellular Fe(II) (17). Interestingly, the two Fur isoforms quantified here appeared to respond to different Fe′ concentrations and may govern "Fe-limited" and "Fe-stressed" conditions, respectively (Fig. 3*A*).

In contrast to the coastal strain, oceanic WH8102 did not show a multitiered proteome response to Fe limitation and lacked many of the Fe response genes discussed above. Oceanic WH8102 lacks flavodoxin, although at least one of its ferredoxin proteins was still regulated by Fe′ levels (*SI Appendix*, Fig. S1). Both WH8102 and WH8020 genomes have more than one ferredoxin isoform that may have different physiological or regulatory roles (*SI Appendix*, Table S1). Additionally, the coastal WH8020 genome contains both ferritin (GenBank accession no. WB44_04810) and heme-based bacterioferritin (GenBank accession no. WB44_10870) (18, 19), whereas oceanic WH8102 lacks both.

This study belies the expectation that oceanic phytoplankton would tend to experience greater Fe stress than coastal phytoplankton (6) for two reasons. First, certain open ocean regions like the southern Sargasso Sea can have relatively high and stable dissolved Fe levels depending on their location (Fig. 1*B*). Second, as we show here, the underlying factor governing Fe acclimation capacity is not Fe availability alone, but the simultaneous pressure exerted by multiple scarce nutrients, in particular N, P, and Fe. The Fe adaptations of coastal WH8020 (relative to WH8102) require P for genome maintenance and N for protein synthesis. These costs can be estimated by examining genomic content and by using quantitative proteomic measurements. Overall, oceanic WH8102 has a ∼10% smaller genome than either coastal strain (WH8020 and CC9311), consistent with the loss of Fe response genes like those encoding ferritin and flavodoxin (Fig. 3*B* and *SI Appendix*, Table S1). This smaller genome likely imparts a selective advantage during P-limited periods in the south Sargasso Sea (20, 21). However, the cost of maintaining a single Fe-adaptive gene within the *Synechococcus* WH8102 genome is only ∼0.04% of the genome P content (1 gene in 2,526 genes total), implying that maintaining each individual gene would incur only a small ecological cost.

The N cost associated with the multitiered Fe-adaptive response in coastal WH8020 was examined using quantitative proteomic methods, where isotopically labeled peptide internal standards were synthesized for ferritin, IdiA, ferredoxin, and flavodoxin, and quantified using multiple reaction monitoring on a quadrupole-orbitrap mass spectrometer (22). N requirements were calculated based on the absolute concentration and chemical formula of each protein (*Materials and Methods*). Ferritin and IdiA synthesis requires ∼3.3–4.4 pmol N per microgram of total protein (Fig. 3*C*). Because the cells must either synthesize ferritin or IdiA depending on ambient Fe concentrations, these Fe-adaptive proteins incur an N cost for the cell regardless of whether Fe levels are high (for Fe storage) or low (for Fe uptake). Flavodoxin has the largest N cost (14.7 pmol N per microgram of total protein; Fig. 3*C*) of the Fe-adaptive proteins targeted here. The ∼100-fold greater abundance of flavodoxin (98.9 fmol per microgram of total protein) compared with ferredoxin (0.73 fmol per microgram of total protein) in WH8020 is consistent with reports of flavodoxin's lower reaction efficiency compared with ferredoxin (23). Whereas flavodoxin only contributes to ∼0.2% of total protein N at its most abundant (0.0019 μg flavodoxin per microgram of total protein), this observation suggests that even the small N costs associated with adaptive responses to nutrient scarcity are ecologically significant, and this is consistent with previous findings of small N cost for adaptive responses to vitamin B_{12} scarcity in diatoms (24). The benefit that flavodoxin imparts in the dynamic coastal ocean likely outweighs the N cost of its synthesis. Moreover, the small N cost of synthesizing Fe-response proteins like flavodoxin is still higher than the P cost of maintaining the corresponding genes.

Our results suggest that the capacity of *Synechococcus* to adapt to Fe limitation therefore depends not on Fe alone, but on the balance between availability of Fe, N, and P. The combination of relatively high dissolved Fe levels (25) and scarcity of N and P in the permanently stratified southern Sargasso Sea may place stronger selective pressure on oceanic WH8102 to eliminate Fe-adaptive genes. A recent North Atlantic transect that sampled near both *Synechococcus* isolation environments illustrates this: oceanic surface waters had elevated Fe:nitrate ratios (11.4:1 pM:nM on average between 64–66°W, the longitude of isolation for WH8102),

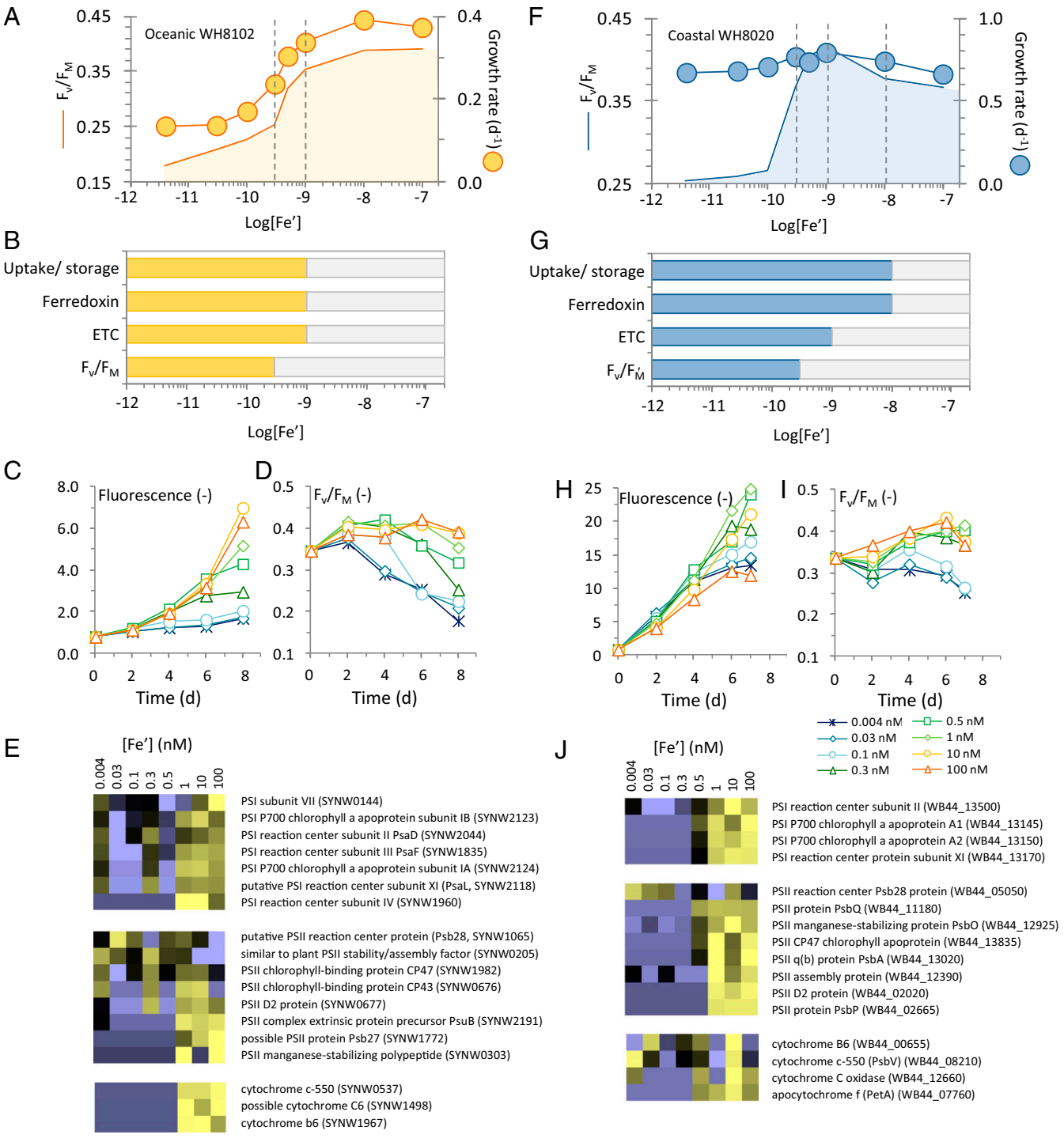

Fig. 2. Physiological and photosynthetic responses of oceanic WH8102 (*Left*, *A–E*) and coastal WH8020 (*Right*, *F–J*) to [Fe′]. Vertical dashed lines in *A* and *F* and bars in *B* and *G* indicate the concentration of Fe′ (plotted as log[Fe′]) at which a given physiological parameter showed a threshold response (*Materials and Methods*). Growth rate (circles) and photosynthetic efficiency (F_v/F_M measured at the time the protein samples were collected, shaded regions) are shown in *A* and *F*. ETC, membrane proteins in the photosynthetic electron transport chain. Growth curves are shown in *C* and *H* and photosynthetic efficiency (Fv/F_M) values collected each day are shown in *D* and *I*. Legend for *C*, *D*, *H*, and *I* is shown below *I*. (*E* and *J*) Heatmap of photosynthetic electron transport chain proteins for *Synechococcus* sp. strains WH8102 (*E*) and WH8020 (*J*). Normalized spectral counts are given in *SI Appendix*, Table S4. Color indicates higher (yellow) or lower (purple) abundance relative to the centered mean value (black).

whereas the Atlantic coast had relatively lower Fe:nitrate (5.3:1 pM:nM at 69°W close to the WH8020 isolation site; Fig. 1*C*). Additionally, oceanic (64–66°W) seawater nitrate:phosphate ratios were low (~2.1:1 nM:nM) relative to both the Redfield ratio (26) (16:1) and WH8102 cell quotas (10.9:1 and 43.8:1 in P-replete and P-limited cultures, respectively) (27). These nutrient availability patterns are consistent with a selection pressure against expending additional N within Fe-adaptive proteins in the oligotrophic southern Sargasso Sea. Specifically, low N levels in the open ocean may make flavodoxin less beneficial for oceanic WH8102, given that

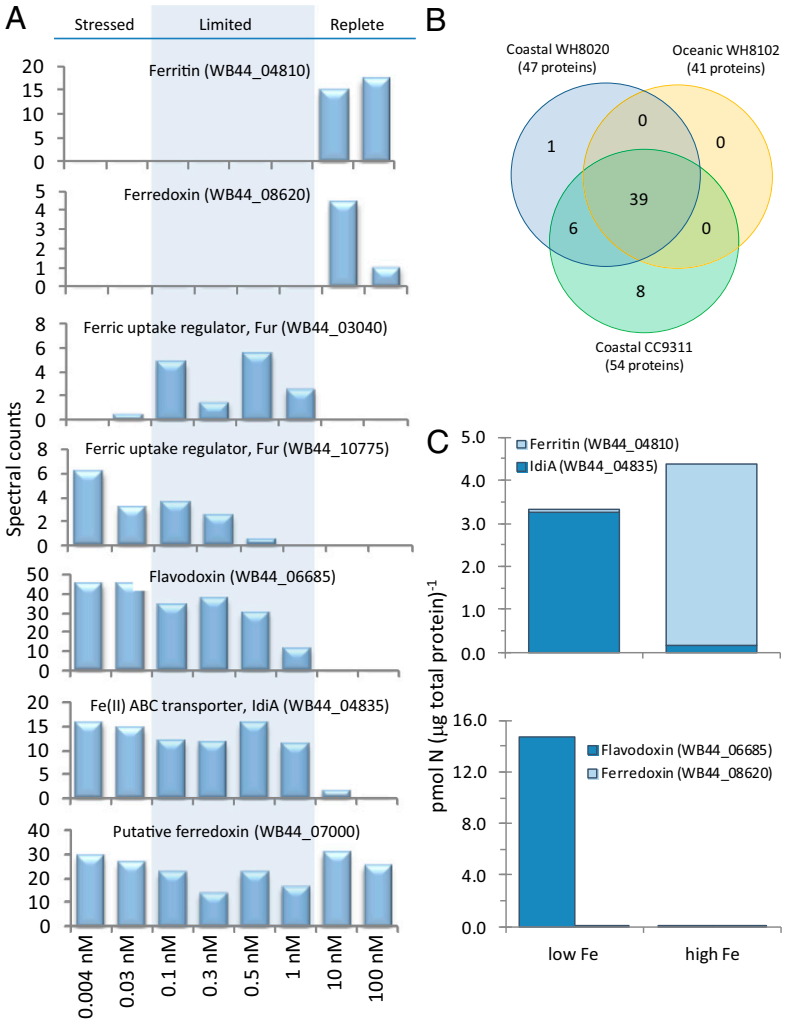

Fig. 3. (*A*) Abundance of Fe-related proteins in coastal *Synechococcus* sp. strain WH8020 in response to [Fe′] (gene IDs correspond to genes in *SI Appendix*, Table S1). (*B*) Venn diagram of Fe response genes (*SI Appendix*, Table S1) in the genomes of oceanic strain WH8102 and coastal strains WH8020 and CC9311. (*C*) N costs associated with Fe response proteins in coastal *Synechococcus* WH8020 under high (>1 nM) and low (≤1 nM) Fe′ conditions (the expression threshold for these proteins). Ferredoxin (GenBank accession no. WB44_08620) was ∼100-fold less abundant than flavodoxin (GenBank accession no. WB44_06685). Although ferredoxin is more abundant under high Fe (see *A*), the effect is masked in *C* due to the scale used for flavodoxin.

less Fe adaptability would be needed under its relatively stable Fe regime (Fig. 1 *B* and *C*). Oceanic WH8102 is likely well suited to these high dust waters, whereas other oceanic strains with greater Fe acclimation capacity may exist in regions with lower Fe availability, such as the Equatorial Pacific (28) and Costa Rica Dome (29), or even seasonally in the northern Sargasso Sea near the Bermuda Atlantic Time Series (BATS; Fig. 1*A*) where dust supply wanes seasonally (9) and Fe is depleted within the deep chlorophyll maximum (30).

In comparison with *Synechococcus*, the N cost of Fe adaptability is apparently not sufficient to deter the highly streamlined *Prochlorococcus* MED4 and MIT9301 genomes from retaining flavodoxin, yet ecotypes adapted to chronic Fe limitation in the Pacific Ocean have eliminated certain Fe-containing genes from their genomes (28). The selective loss of Fe-containing proteins (but not Fe-free Fe response proteins like flavodoxin) from *Prochlorococcus* genomes implies a particular importance of adapting to Fe scarcity in *Prochlorococcus*. *Prochlorococcus* has approximately twofold lower cellular N requirements than *Synechococcus* (27), and obtains N from urea (31, 32). As a result, *Synechococcus* may experience greater selective pressure to conserve N, given that smaller *Prochlorococcus*, with its larger surface area-to-volume ratio, would likely outcompete *Synechococcus* for Fe in either case.

These results demonstrate distinct responses of marine *Synechococcus* from coastal and open Atlantic Ocean environments. The surprising dynamic, multitiered Fe response of coastal *Synechococcus* WH8020 implies that periods of Fe scarcity likely extend well into the coastal zones of continental shelf regions, in addition to the open ocean and coastal upwelling systems. The limited response of oceanic *Synechococcus* WH8102 demonstrates the challenge of multinutrient scarcity in the open ocean, where the advantages of maintaining Fe adaptability are offset by even small nutritional costs. These responses suggest that the need to conserve Fe plays an important role in species evolution in the coastal and open ocean, but the outcome rests on a complex interplay between the availability of multiple scarce nutrients and an organism's complement of biochemical responses.

Materials and Methods

Strains and Culturing Conditions. *Synechococcus* sp. strain WH8102 was isolated from surface waters in the oligotrophic southern Sargasso Sea (22.495°N, 65.6°W by F. Valois and J. Waterbury) north of Puerto Rico, where the waters are permanently stratified, and belongs to *Synechococcus* clade III (2). Strain WH8020 was isolated from surface waters near Woods Hole, MA (38.68°N, 69.32°W by

F. Valois and J. Waterbury). Both strains were generously provided by the Waterbury laboratory. The WH8102 genome is available at www.ncbi.nlm.nih.gov/Taxonomy/Browser/wwwtax.cgi?id=84588. The WH8020 genome reported in this paper has been deposited in the GenBank BioProject database (accession no. PRJNA278997).

Synechococcus spp. WH8102 and WH8020 were cultured at 23 °C under 10 μmol quanta $m^{-2}{\cdot}s^{-1}$ constant white light provided by a mixture of fluorescent cool white and grow light bulbs. Microwave sterilized media was based on a modified SN media recipe for trace metal cultivation and consisted of oligotrophic seawater diluted 25% with MilliQ water and amended with nutrients and trace metals: 2 mM $NaNO_3$, 0.2 mM NH_4Cl, 140 μM K_2HPO_4, 100 μM Na_2CO_3, 10 μM EDTA disodium salt, 1.42 μM $MnCl_2$, 0.32 μM Na_2MoO_4, 0.15 μM $ZnSO_4$, 0.17 μM $Co(NO_3)_2$, and 6.5 μM citric acid. The seawater was collected on the CoFeMUG Cruise in 2007 from the mid-Atlantic Ocean and had a total Fe concentration of 0.1 nM at the time of collection (33). Given the 10 μM EDTA added to the media, this background contributed 0.004 nM Fe′ to the overall Fe′ content. Additional Fe was added back to the seawater as $FeCl_3$ at various concentrations described below.

To induce iron limitation, cells were transferred successively into fresh no-Fe-added media that contained all other media components until growth limitation was observed. FIRe fluorescence was monitored to determine when stationary phase was reached based on raw fluorescence growth curves and F_v/F_M values (see FIRe methods below). Cells were maintained under these Fe-limited stationary conditions for at least 2 wk. The Fe-limited parent culture was then used to inoculate eight new single-replicate flasks containing 200 mL of fresh medium. The Fe concentrations added to these flasks were 2,533, 253, 25, 13, 7, 3, 0.7, and 0 nM total $FeCl_3$ from a single stock prepared fresh in weakly acidified MilliQ water, and all culture flasks had 10 μM EDTA regardless of the concentration of Fe added. Iron concentrations were measured using a coastal seawater method (34) on an inductively coupled plasma mass spectrometer (Thermo iCAP Q ICP-MS) for the two most concentrated batches of media, where the second was a 10-fold dilution of the first. The values (2,645 ± 198 nM, coefficient of variation = 0.075; and 2,420 ± 14 nM, coefficient of variation = 0.059, value accounts for the 10-fold dilution of this sample) were averaged (2,533 nM), and this value was used to calculate the iron dilutions to all treatments as described above. Adding the background concentration in the seawater (0.1 nM total Fe) provides the total iron concentration in the lower iron concentration treatments.

The sum of inorganic iron species (Fe′) was estimated using a factor of Fe'/Fe_{Total} = of 0.039, based on empirical determination of the FeEDTA dissociation constant and resultant Fe′ in seawater media with an equivalent 10 μM EDTA in darkness at 20 °C (35). This yielded free Fe′ concentrations of 100, 10, 1, 0.5, 0.3, 0.1, 0.03, and 0.004 nM, respectively. Constants and values for Fe′ in light were also available (Fe'/Fe_{Total} = 0.065) (35), but because the illumination used was much stronger than that of this experiment (10 versus 500 μmol quanta $m^{-2}{\cdot}s^{-1}$), the dark results seem more representative of our experimental system. The background Fe′ concentration in the no-Fe-added seawater was 0.004 nM. The Fe′ value is the amount considered to be easily accessible to iron transport systems, whereas organically chelated iron (FeEDTA or natural iron ligands) (36) may be accessible through reductase or siderophore transport systems. No organic chelated iron acquisition systems are currently identified in marine *Synechococcus*.

FIRe fluorescence (F_v/F_M, see below) was monitored daily. Cultures for protein analysis were harvested during late log phase by gentle vacuum filtration onto 0.2-μm Supor filters and frozen at −80 °C until processing.

Protein Extraction and Digestion. Frozen cell samples for protein extraction were rinsed from the filters in 100 mM ammonium bicarbonate, sonicated on ice a minimum of 10 min to lyse cells and break up cellular membranes, and centrifuged to pellet cell debris. Proteins in the supernatant were precipitated overnight in 100% (vol/vol) acetone at −20 °C. The pellet was resuspended in 6 M urea with 0.1 mM ammonium bicarbonate, reduced with 10 mM DTT in a thermomixer (56 °C, 450 rpm, 1 h), and alkylated with 30 mM iodoacetamide (20 °C on bench for 1 h). Proteins were then digested with trypsin (Promega Trypsin Gold; 37 °C, 400 rpm overnight in a thermomixer) at an enzyme:protein ratio of 1:50. The tryptic peptides were concentrated by evaporation and resuspended in 2% (vol/vol) acetonitrile with 0.2% formic acid.

Global Proteome Analysis. Chromatography and tandem mass spectrometry (LC-MS/MS) of the tryptic peptides was performed on a Q Exactive (QE) Orbitrap mass spectrometer (Thermo Scientific). Chromatography was performed using a 180-min nonlinear gradient of 0.1% formic acid in water and 0.1% formic acid in acetonitrile on a 25 cm × 100 μm column (New Objective PicoTip emitter PicoFrit) packed with 3 μm C18 silica packing material (Reprosil-Gold 120 C18, 3 μm; Dr. Maisch GmbH). Tandem mass spectrometry was performed on the top 15 ions. Full MS scans were performed at 70k resolution with a scan range of 380–2,000 *m/z* and 1e6 AGC target. Data-dependent MS2 scans were monitored at 17.5k resolution with 1e5 AGC target, 100 ms maximum injection time, and a 2.0 *m/z* isolation window.

Proteins were identified against the genome for each strain using the SEQUEST algorithm within Proteome Discoverer (Thermo) and normalized spectral counts tabulated in Scaffold software (version 4.3.2 Proteome Software). Protein identification criteria included a protein identification probability of 99%, a peptide identification probability of 95%, and identification of two or more peptides from the protein's sequence using the Peptide Prophet algorithm (37). Relative protein abundance data were normalized to total spectral counts. The global data were then imported into Cluster 3.0 (38), log transformed, centered on mean, and normalized across treatments to create a heatmap (Fig. 2). Proteins were clustered using the correlation (uncentered) similarity metric and centroid linkage options.

The global proteome values show the spectral counts for each protein, which are uncalibrated measurements of relative abundance for which comparisons within a protein across treatments is the best application. In contrast, the targeted calibrated measurements for which isotopically labeled peptide standards are used (see below), are the appropriate measurement for comparisons of concentrations of different proteins.

Targeted Protein Quantitation. Peptide target sequences representing proteins of interest were identified from peptides in the global proteome. Two or more peptides per protein of interest were synthesized using SpikeTides Synthetic Proteotypic Peptides (JPT Peptide Technologies GmbH). These peptide standards are labeled with trypsin-cleavable stable isotope markers ("heavy" peptides), allowing precise quantitation of the peptide. Experimental samples were spiked with known amounts of each standard to determine the amount of the respective protein in the sample on a femtomole peptide/microgram total protein basis. Samples were analyzed using parallel reaction monitoring (PRM) (see *SI Appendix*, Table S4 for settings) (39, 40), where each precursor ion (light and heavy masses) was selected by the quadrupole, fragmented, and then all fragment ions were quantified in the orbitrap (22). The sum of the top five fragment ion intensities was calculated in Skyline (MacCoss Lab Software version 3.1) and used to estimate peptide signal intensity. Peptide concentration was calculated based on the ratio to the heavy peptide standards that were added in known quantity.

To compare the amount of protein under Fe replete and deplete conditions, all PRM values above (replete) and below (deplete) the Fe threshold for that protein were averaged and compared for both peptides per targeted protein (*SI Appendix*, Table S2). For example, for flavodoxin the threshold for WH8020 occurred for cells grown between 1 and 10 nM, so all protein concentrations for cells grown at ≥10 nM were averaged to obtain the replete, or "high" protein concentration, and all values for cells grown at ≤1 nM were averaged to obtain the deplete, or "low" protein concentration. The replete and deplete values were subtracted to determine the mass of extra protein produced by the cell when these genes are expressed. The N cost associated with each protein was calculated based on the number of N atoms per protein for each target.

Fe Response Gene Identification. The WH8102 and CC9311 genome annotations were searched using iron-related key words and for known iron-sparing proteins. The identified genes were used to BLAST the WH8020 genome to identify orthologous genes.

Photosystem II Fluorescence. Photosystem II fluorescence was measured using a FIRe fluorometer with FIReview software (Satlantic) and blue excitation light (450 nm with 30 nm bandwidth). Due to the small cross section of *Synechococcus* for blue light, it is necessary to increase the duration of the saturating flash beyond the default value to ensure that a steady state fluorescence plateau is reached; in this study, a single turnover flash duration of 200 μs was used. Default values were used for all other parameters. The reference excitation profile was recorded for these timing parameters using rose bengal dye. The fluorescence parameters F_v/F_M (photosynthetic efficiency in the dark-adapted state) were determined using the curve fitting program in FIRePro with the relaxation kinetics fitting disabled. The F_v/F_M of each culture was monitored daily following readdition of Fe to the WH8102 and WH8020 cultures.

Growth Curves. Doubling times in Fig. 2 *A* and *F* were calculated from fluorescence growth curves shown in Fig. 2 *C* and *H* using the equation $T_d = [(t_f - t_i)\ln 2]/[\ln(c_f/c_i)]$, where T_d is the time for the population to double, t_f is final time, t_i is initial time, c_f is the final concentration, and c_i is the initial concentration. Fluorescence trends were confirmed against flow cytometry measurements of samples taken on the final time point of each experiment (*SI Appendix*, Fig. S2). Formalin fixed samples were flash frozen in liquid nitrogen and stored frozen at −80 °C until analysis on

an Accuri flow cytometer. Counts were triggered on chlorophyll fluorescence. These data are shown in *SI Appendix*, Fig. S2, and $R^2 = 0.94$.

Threshold response calculations. For Fig. 2, protein thresholds were determined as the concentration at which the protein declined to 50% of its maximal value. Photophysiological thresholds were taken as the concentration above which the F_v/F_M response diverged from the "no iron added" condition.

Nutrient and dissolved Fe concentrations. Seawater samples for Fe concentration analysis were collected on US GEOTRACES section GA03 using trace-metal clean sampling protocols (41). Fe concentrations were analyzed on a Neptune multicollector ICP-MS at the University of South Carolina by isotope dilution, after concentrating and purifying Fe from a 1-L seawater samples (42, 43). Nanomolar concentrations of dissolved phosphate, nitrate, and nitrite were determined on board ship using conventional automated nutrient analyzer methods modified for the use of 250-cm-long liquid core waveguides as described previously (44, 45).

ACKNOWLEDGMENTS. We are grateful to John Waterbury and Frederica Valois for helpful discussions and culture strains, and Madeli Castruita for discussion on bacterioferritin sequences. This work was supported by a National Science Foundation Postdoctoral Research Fellowship in Biology (to K.R.M.M.) (NSF 1103575); National Science Foundation Oceanography Grants OCE-1220484, OCE-0928414, OCE-1233261, OCE-1155566, OCE-1131387, and OCE-0926092; as well as Gordon and Betty Moore Foundation Grants 3782 and 3934.

1. Flombaum P, et al. (2013) Present and future global distributions of the marine Cyanobacteria Prochlorococcus and Synechococcus. *Proc Natl Acad Sci USA* 110(24): 9824–9829.
2. Scanlan DJ, et al. (2009) Ecological genomics of marine picocyanobacteria. *Microbiol Mol Biol Rev* 73(2):249–299.
3. Moore CM, et al. (2013) Processes and patterns of oceanic nutrient limitation. *Nat Geosci* 6(9):701–710.
4. Palenik B, et al. (2003) The genome of a motile marine Synechococcus. *Nature* 424(6952):1037–1042.
5. Palenik B, et al. (2006) Genome sequence of Synechococcus CC9311: Insights into adaptation to a coastal environment. *Proc Natl Acad Sci USA* 103(36):13555–13559.
6. Sunda WG, Swift DG, Huntsman SA (1991) Low iron requirement for growth in oceanic phytoplankton. *Nature* 351(6321):55–57.
7. Peers G, Price NM (2006) Copper-containing plastocyanin used for electron transport by an oceanic diatom. *Nature* 441(7091):341–344.
8. Mahowald NM, et al. (2005) Atmospheric global dust cycle and iron inputs to the ocean. *Glob Biogeochem Cycles* 19(4):GB4025.
9. Prospero JM, et al. (1996) in *Nitrogen Cycling in the North Atlantic Ocean and its Watersheds*, ed Howarth RW (Springer, Amsterdam), pp 27–73. Available at link.springer.com/chapter/10.1007/978-94-009-1776-7_2.
10. Biller DV, Bruland KW (2014) The central California Current transition zone: A broad region exhibiting evidence for iron limitation. *Prog Oceanogr* 120:370–382.
11. Mackey KRM, Chien C-T, Paytan A (2014) Microbial and biogeochemical responses to projected future nitrate enrichment in the California upwelling system. *Front Microbiol* 5:632.
12. Hunter-Cevera KR (2014) Population dynamics and diversity of Synechococcus on the New England Shelf (Massachusetts Institute of Technology, Cambridge, MA). Available at dspace.mit.edu/handle/1721.1/92591.
13. Wu J, Luther GW (1996) Spatial and temporal distribution of iron in the surface water of the northwestern Atlantic Ocean. *Geochim Cosmochim Acta* 60(15):2729–2741.
14. Webb EA, Moffett JW, Waterbury JB (2001) Iron stress in open-ocean cyanobacteria (Synechococcus, Trichodesmium, and Crocosphaera spp.): Identification of the IdiA protein. *Appl Environ Microbiol* 67(12):5444–5452.
15. Allen AE, et al. (2008) Whole-cell response of the pennate diatom Phaeodactylum tricornutum to iron starvation. *Proc Natl Acad Sci USA* 105(30):10438–10443.
16. La Roche J, Boyd PW, McKay RML, Geider RJ (1996) Flavodoxin as an in situ marker for iron stress in phytoplankton. *Nature* 382(6594):802–805.
17. Escolar L, Pérez-Martín J, de Lorenzo V (1999) Opening the iron box: Transcriptional metalloregulation by the Fur protein. *J Bacteriol* 181(20):6223–6229.
18. Dautant A, et al. (1998) Structure of a monoclinic crystal from of cyctochrome b1 (Bacterioferritin) from E. coli. *Acta Crystallogr D Biol Crystallogr* 54(Pt 1):16–24.
19. Castruita M, et al. (2006) Overexpression and characterization of an iron storage and DNA-binding Dps protein from Trichodesmium erythraeum. *Appl Environ Microbiol* 72(4):2918–2924.
20. Wu J, Sunda W, Boyle EA, Karl DM (2000) Phosphate depletion in the western North Atlantic Ocean. *Science* 289(5480):759–762.
21. Coleman ML, Chisholm SW (2010) Ecosystem-specific selection pressures revealed through comparative population genomics. *Proc Natl Acad Sci USA* 107(43): 18634–18639.
22. Gallien S, et al. (2012) Targeted proteomic quantification on quadrupole-orbitrap mass spectrometer. *Mol Cell Proteomics* 11(12):1709–1723.
23. Fitzgerald MP, Rogers LJ, Rao KK, Hall DO (1980) Efficiency of ferredoxins and flavodoxins as mediators in systems for hydrogen evolution. *Biochem J* 192(2):665–672.
24. Bertrand EM, et al. (2013) Methionine synthase interreplacement in diatom cultures and communities: Implications for the persistence of B12 use by eukaryotic phytoplankton. *Limnol Oceanogr* 58(4):1431–1450.
25. Bergquist BA, Boyle EA (2006) Dissolved iron in the tropical and subtropical Atlantic Ocean. *Glob Biogeochem Cycles* 20(1):GB1015.
26. Martiny AC, et al. (2013) Strong latitudinal patterns in the elemental ratios of marine plankton and organic matter. *Nat Geosci* 6(4):279–283.
27. Bertilsson S, Berglund O, Karl DM, Chisholm SW (2003) Elemental composition of marine Prochlorococcus and Synechococcus: Implications for the ecological stoichiometry of the sea. *Limnol Oceanogr* 48(5):1721–1731.
28. Rusch DB, Martiny AC, Dupont CL, Halpern AL, Venter JC (2010) Characterization of Prochlorococcus clades from iron-depleted oceanic regions. *Proc Natl Acad Sci USA* 107(37):16184–16189.
29. Ahlgren NA, et al. (2014) The unique trace metal and mixed layer conditions of the Costa Rica upwelling dome support a distinct and dense community of Synechococcus. *Limnol Oceanogr* 59(6):2166–2184.
30. Sedwick PN, et al. (2005) Iron in the Sargasso Sea (Bermuda Atlantic time-series study region) during summer: Eolian imprint, spatiotemporal variability, and ecological implications. *Glob Biogeochem Cycles* 19(4):GB4006.
31. Saito MA, et al. (2014) Multiple nutrient stresses at intersecting Pacific Ocean biomes detected by protein biomarkers. *Science* 345(6201):1173–1177.
32. Casey JR, Lomas MW, Mandecki J, Walker DE (2007) Prochlorococcus contributes to new production in the Sargasso Sea deep chlorophyll maximum. *Geophys Res Lett* 34(10):L10604.
33. Noble AE, et al. (2012) Basin-scale inputs of cobalt, iron, and manganese from the Benguela-Angola front to the South Atlantic Ocean. *Limnol Oceanogr* 57(4): 989–1010.
34. Field MP, Cullen JT, Sherrell RM (1999) Direct determination of 10 trace metals in 50 mL samples of coastal seawater using desolvating micronebulization sector field ICP-MS. *J Anal Spectrom* 14(9):1425–1431.
35. Sunda W, Huntsman S (2003) Effect of pH, light, and temperature on Fe–EDTA chelation and Fe hydrolysis in seawater. *Mar Chem* 84(1-2):35–47.
36. Lis H, Kranzler C, Keren N, Shaked Y (2015) A comparative study of iron uptake rates and mechanisms amongst marine and fresh water cyanobacteria: Prevalence of reductive iron uptake. *Life (Basel)* 5(1):841–860.
37. Keller A, Nesvizhskii AI, Kolker E, Aebersold R (2002) Empirical statistical model to estimate the accuracy of peptide identifications made by MS/MS and database search. *Anal Chem* 74(20):5383–5392.
38. de Hoon MJL, Imoto S, Nolan J, Miyano S (2004) Open source clustering software. *Bioinformatics* 20(9):1453–1454.
39. Saito MA, et al. (2011) Iron conservation by reduction of metalloenzyme inventories in the marine diazotroph Crocosphaera watsonii. *Proc Natl Acad Sci USA* 108(6): 2184–2189.
40. Lange V, et al. (2008) Targeted quantitative analysis of Streptococcus pyogenes virulence factors by multiple reaction monitoring. *Mol Cell Proteomics* 7(8):1489–1500.
41. Cutter GA, Bruland KW (2012) Rapid and noncontaminating sampling system for trace elements in global ocean surveys. *Limnol Oceanogr Methods* 10(6):425–436.
42. Conway TM, Rosenberg AD, Adkins JF, John SG (2013) A new method for precise determination of iron, zinc and cadmium stable isotope ratios in seawater by double-spike mass spectrometry. *Anal Chim Acta* 793:44–52.
43. Conway TM, John SG (2014) Quantification of dissolved iron sources to the North Atlantic Ocean. *Nature* 511(7508):212–215.
44. Zimmer LA, Cutter GA (2012) High resolution determination of nanomolar concentrations of dissolved reactive phosphate in ocean surface waters using long path liquid waveguide capillary cells (LWCC) and spectrometric detection. *Limnol Oceanogr Methods* 10(8):568–580.
45. Zhang J-Z (2000) Shipboard automated determination of trace concentrations of nitrite and nitrate in oligotrophic water by gas-segmented continuous flow analysis with a liquid waveguide capillary flow cell. *Deep Sea Res Part Oceanogr Res Pap* 47(6): 1157–1171.

Supplemental Information

Figure S1: Abundance of Fe related proteins in oceanic *Synechococcus sp*. strain WH8102 in response to [Fe'].

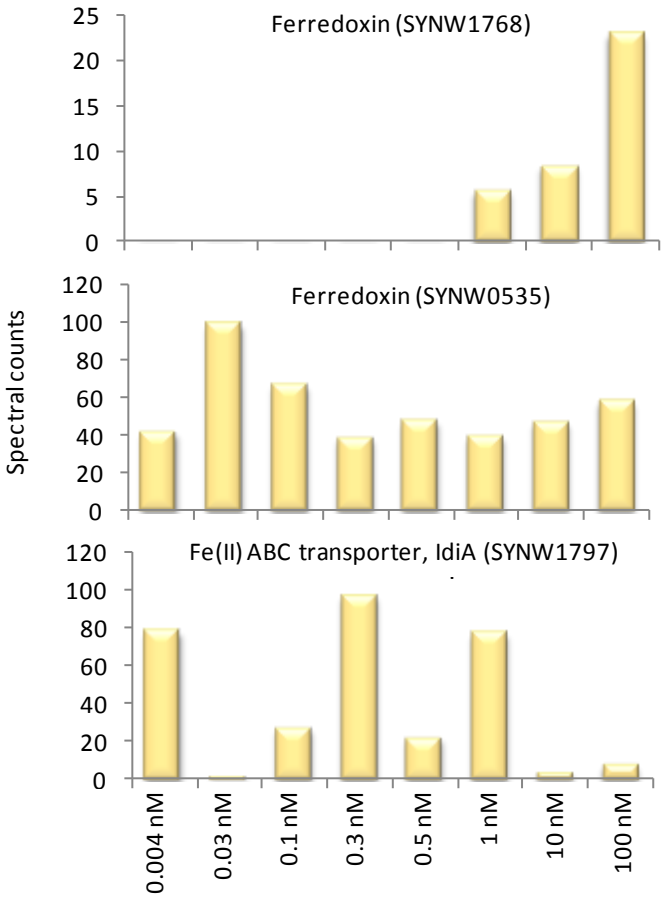

Figure S2: Comparison of flow cytometry and fluorescence measurements on the final day of each experiment.

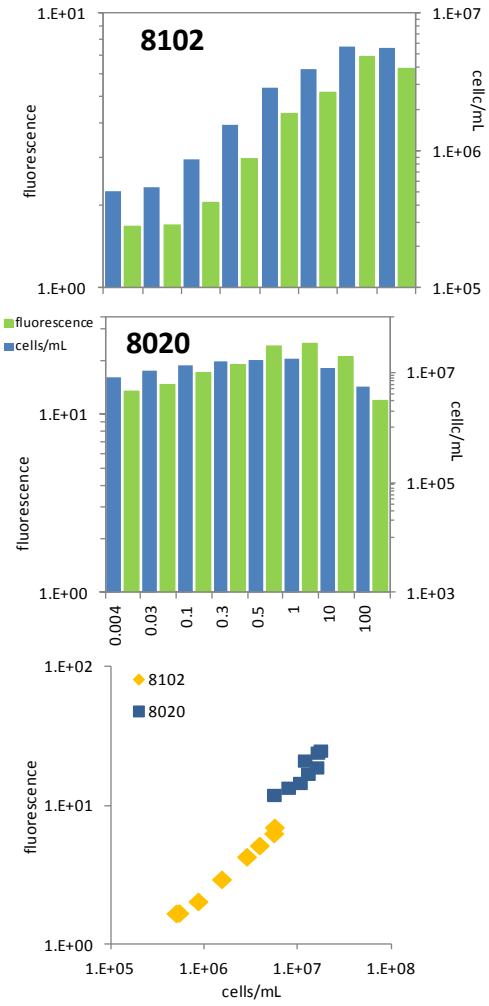

:

Table S1: Fe related proteins in the *Synechococcus* WH8020, WH8102, and CC9311 genomes. Proteins listed in each row represent the closest matching amino acid sequences among the three strains. Black, green, and blue text indicates that the protein in a given row is present in three, two, or one of the strain genomes respectively. This information is shown graphically in the Venn diagram in figure 3B.

WH8102		WH8020		CC9311	
ID	Protein	ID	Protein	ID	Protein
SYNW1841	Cytochrome b6/f complex subunit (Rieske iron-sulfur protein	WB44_07765	Cytochrome b6-f complex iron-sulfur subunit PetC1 (Rieske iron sulfur protein EC 1.10.99.1)	sync_2149	cytochrome b6-f complex iron-sulfur subunit
SYNW1632	hypothetical	WB44_00870	Possible 4Fe-4S iron sulfur cluster binding protein	sync_0748	4Fe-4S iron sulfur cluster binding protein
SYNW1705	hypothetical	WB44_01950	Ferredoxin	sync_0892	ferredoxin
SYNW1277	ferredoxin		Ferredoxin	sync_1397	iron-sulfur cluster-binding protein
SYNW1768	ferredoxin	WB44_07000	Ferredoxin	sync_2017	iron-sulfur cluster-binding protein
SYNW0624	possible 3Fe-4S ferredoxin	WB44_08620	Ferredoxin	sync_2348	ferredoxin (3Fe-4S)
SYNW1981	ferredoxin	WB44_13840	Ferredoxin	sync_0535	ferredoxin (2Fe-2S)
SYNW0697	putative ferredoxin like protein	WB44_02125	Ferredoxin, 2Fe-2S	sync_0919	ferredoxin
SYNW1343	ferredoxin	WB44_02385	soluble [2Fe-2S] ferredoxin	sync_0980	ferredoxin
SYNW1274	Ferredoxin	WB44_04140	soluble [2Fe-2S] ferredoxin	sync_1394	ferredoxin (2Fe-2S)
		WB44_06700	soluble [2Fe-2S] ferredoxin	sync_1953	ferredoxin

SYNW0535	Ferredoxin	WB44_08230	soluble [2Fe-2S] ferredoxin	sync_2254	ferredoxin
SYNW0497	Ferredoxin	WB44_08440	soluble [2Fe-2S] ferredoxin	sync_2310	ferredoxin, 2Fe-2S
		WB44_10810	soluble [2Fe-2S] ferredoxin	sync_2841	ferredoxin
SYNW0521	putative ferredoxin-thioredoxin reductase, variable chain	WB44_08310	Ferredoxin-thioredoxin reductase, variable chain	sync_2274	ferredoxin-thioredoxin reductase variable chain
SYNW0318	Ferredoxin thioredoxin reductase, catalytic beta chain	WB44_09225	Ferredoxin	sync_2484	ferredoxin thioredoxin reductase, catalytic beta chain
SYNW0751	ferredoxin--NADP reductase	WB44_02485	Ferredoxin-NADP(+) reductase (EC 1.18.1.2)	sync_1003	ferredoxin--NADP reductase
SYNW2132	Ferredoxin-dependent glutamate synthase	WB44_13115	Ferredoxin-dependent glutamate synthase (EC 1.4.7.1)	sync_0387	ferredoxin-dependent glutamate synthase
SYNW2477	Ferredoxin--nitrite reductase	WB44_11090	Ferredoxin--nitrite reductase (EC 1.7.7.1)	sync_2898	ferredoxin-nitrite reductase
SYNW1095	Ferredoxin-sulfite reductase	WB44_03570	Ferredoxin--sulfite reductase (EC 1.8.7.1)	sync_1280	sulfite reductase subunit beta
		WB44_11855	Ferredoxin reductase		
SYNW1797	putative iron ABC transporter, substrate binding protein	WB44_04835	Ferric iron ABC transporter, iron-binding protein	sync_1545	ABC-type Fe3+ transport system periplasmic component
SYNW1798	putative iron ABC transporter	WB44_07150	Ferric iron ABC transporter, permease protein	sync_2048	ABC-type Fe3+ transport system permease component
SYNW1544	ABC transporter, ATP binding component, possibly iron transporter	WB44_06655	ABC transporter, ATP binding component, possibly iron transporter	sync_1942	ABC transporter ATP-binding protein

				sync_0682	ferrous iron transport protein A
				sync_0681	ferrous iron transport protein B
				sync_2395	iron ABC transporter ATP-binding protein
SYNW1340	ABC transporter, ATP binding domain, possibly Mn transporter	WB44_05820	ABC transporter, ATP binding domain, possibly Mn transporter	sync_1757	iron chelate ABC transporter ATP-binding protein
SYNW2366	conserved hypothetical putative integralmembrane protein	WB44_10525	Mn2+ and Fe2+ transporter, NRAMP family	sync_2773	Mn2+/Fe2+ transporter
		WB44_04810	Ferritin	sync_1539	Ferritin
				sync_0687	Ferritin
				sync_0854	Ferritin
				sync_1077	Ferritin
				sync_0680	Ferritin
SYNW1747	ferrochelatase	WB44_06915	Ferrochelatase, protoheme ferro-lyase (EC 4.99.1.1)	sync_2000	ferrochelatase
SYNW0865	Ferric uptake regulator family	WB44_03040	Ferric uptake regulation protein FUR	sync_1167	transcriptional regulator, Fur family protein
SYNW0774	Ferric uptake regulation protein	WB44_05660	Peroxide stress regulator; Ferric uptake regulation protein; Fe2+/Zn2+ uptake regulation proteins	sync_1722	transcriptional regulator, Fur family protein
SYNW2401	Ferric uptake regulator family	WB44_10775	Ferric uptake regulation protein	sync_2831	transcriptional regulator, Fur family protein

		WB44_06685	Flavodoxin 1	sync_1950	flavodoxin FldA
SYNW2368	putative flavoprotein	WB44_10555	Diflavin flavoprotein SYNW2368	sync_2780	flavodoxin:flavin reductase-likedomain-containing protein
SYNW0163	putative glycolate oxidase subunit (Fe-S)	WB44_12240	Glycolate dehydrogenase (EC 1.1.99.14), iron-sulfur subunit GlcF	sync_0213	Fe-S oxidoreductase
				sync_2669	Iron-containing alcohol dehydrogenase
		WB44_04570	Iron-regulated protein A precursor	sync_1502	Iron-regulated protein A precursor, putative
SYNW0321	ABC transporter, membrane component	WB44_09210	Iron-sulfur cluster assembly protein SufD	sync_2481	FeS assembly protein SufD
SYNW0320	ABC transporter, ATP-binding component	WB44_09215	Iron-sulfur cluster assembly ATPase protein SufC	sync_2482	FeS assembly ATPase SufC
SYNW0319	ABC transporter, membrane component	WB44_09220	Iron-sulfur cluster assembly protein SufB	sync_2483	cysteine desulfurase activator complex subunit SufB
SYNW0317	ArsR family transcriptional regulator	WB44_09230	Iron-sulfur cluster regulator SufR	sync_2485	iron-sulfur cluster biosynthesis transcriptional regulator SufR
SYNW0712	possible sufE protein	WB44_02220	Sulfur acceptor protein SufE for iron-sulfur cluster assembly	sync_0942	Fe-S metabolism protein, SufE family protein
SYNW0007	hypothetical protein	WB44_11325	FIG01150787: hypothetical protein	sync_0007	iron-sulfur cluster binding protein, putative
SYNW2479	ABC transporter component, possibly Zn	WB44_04545	manganese/zinc/iron chelate ABC transporter (MZT) family, permease	sync_1497	manganese/zinc/iron chelate ABC transporter permease

			protein		
SYNW2480	ABC transporter,ATP binding component, possibly zinc transport	WB44_04550	ABC transporter,ATP binding component, possibly zinc transport	sync_1498	manganese/zinc/iron chelate ABC transporter ATP-binding protein
SYNW2214	hypothetical protein	WB44_09615	probable iron binding protein from the HesB_IscA_SufA family	sync_2569	iron-sulfur cluster assembly accessory protein
SYNW1990	hypothetical protein	WB44_13800	Putative heme iron utilization protein	sync_0526	hypothetical protein
		WB44_10870	Non-specific DNA-binding protein Dps / Iron-binding ferritin-like antioxidant protein / Ferroxidase	sync_2856	hypothetical protein

Table S2: Stoichiometric calculations of iron responsive proteins in WH8020. The quantitation is based on the average of all measurements for each peptide standard. "Low Fe" values are averages of all measurements ≤1nM Fe', while "high Fe" values are averages of all measurements >1nM Fe'. The molecular weight and number of N atoms per protein are based on amino acid sequences for each protein.

Protein	Peptide standard target sequences	Protein molecular weight (fg / fmol)	N atoms per protein (fmol N / fmol)	Target protein abundance "Low Fe" (fmol / μg total protein)	Target protein abundance "High Fe" (fmol / μg total protein)	Difference in fmol between "high" and "low" treatments (fmol / μg total protein)	Difference in fg between "high" and "low" treatments (fg / μg total protein)	Difference in percent between "high" and "low" treatments* (%)	N content "Low Fe" (pmol N/ ug total protein)	N content "High Fe" (pmol N/ ug total protein)
IdiA (1196)	ADVIILVDAAR, LVEASGISLVQR, GLTSNVSQPYFGGDIGLIR	35907	457	7.14	0.39	6.76	242585	0.024	3.27	0.18
Ferritin (1188)	SQSNDLQALDAPR, FANGDPTALLVIDNELR	20138	244	0.28	17.25	16.97	341713	0.034	0.068	4.21

Flavodoxin (1628)	DLLPGTETK, VPTDGYTFAESK	18829	149	98.88	0.038	98.84	1861086	0.19	14.73	0.0056
Ferredoxin (2042)	SGAVEQPDAMGVK, ADGFTLLCVAFPCSDLR	13057	153	0.73	0.29	0.44	5745	0.00057	0.11	0.044

* Difference in percent is calculated as the difference in protein under high and low Fe conditions (in μg) divided by the total protein (in μg) multiplied by 100.

Table S3: Nutrient data from GEOTRACES cruise GT11. For samples collected via geofish, dissolved nitrate and phosphate data were selected based on the nearest sampling station to the dissolved iron sample site (less than 0.2 degrees latitude difference).

Station number	Collection method	latitude (degrees)	longitude (degrees)	nitrate (nM)	phosphate (nM)	dissolved Fe (nM)
1	Go-Flo, 30 m	39.700°N	-69.808°W	734.1	69.8	0.51
2	Go-Flo, 35 m	39.350 °N	-69.541 °W	83	58.2	0.54
3	Go-Flo, 28 m	38.690 °N	-69.060 °W	81.6	16.1	0.43
6	Go-Flo, 41 m	37.580 °N	-68.437 °W	22.9	16.3	0.31
8	Go-Flo, 32 m	35.420 °N	-66.534 °W	43.3	19.6	0.38
10	Go-Flo, 40 m	31.750 °N	-64.170 °W	29.77	14.5	0.42
12	Go-Flo, 41 m	29.700 °N	-56.810 °W	52.3	9.3	0.62
14	Go-Flo, 41 m	27.580 °N	-49.630 °W	45.4	7.2	0.87
16	Go-Flo, 41 m	26.136 °N	-44.820 °W	30	7.9	0.8
18	Go-Flo, 40 m	24.150 °N	-40.210 °W	81.3	11	0.54
20	Go-Flo, 41 m	22.333 °N	-35.870 °W	71.9	8.9	0.48
22	Go-Flo, 51 m	19.433 °N	-29.380 °W	27.1	9.9	0.35
24	Go-Flo, 40 m	17.400 °N	-24.500 °W	209.3	21.6	0.39
1	Geofish, mixed layer	39.693 °N	-69.808 °W	734.1	69.8	0.65
2	Geofish, mixed layer	39.350 °N	-69.541 °W	83.0	58.2	0.75
8	Geofish, mixed layer	35.420 °N	-66.534 °W	43.3	19.6	1.18
10	Geofish, mixed layer	31.750 °N	-64.17 °W	29.8	14.5	0.45
12	Geofish, mixed layer	29.700 °N	-56.817 °W	52.3	9.3	0.62
14-15	Geofish, mixed layer	27.583 °N	-49.693 °W	59.1	6.7	0.89
16-17	Geofish, mixed layer	26.137 °N	-44.826 °W	45.2	9.5	0.74
18-19	Geofish, mixed layer	24.150 °N	-40.218 °W	34.3	10.3	0.48
22-23	Geofish, mixed layer	19.433 °N	-29.383 °W	45.5	13.6	0.32
23-24	Geofish, mixed layer	17.400 °N	-24.500 °W	47.9	18.5	0.32

Table S4: Parallel reaction monitoring conditions for targeted natural abundance peptides and isotopically labeled peptide standards.

Protein	Peptide standard target sequences	Natural abundance mass (m/z)	Isotopically-labeled standard mass (m/z)
IdiA (1196)	ADVIILVDAAR, LVEASGISLVQR, GLTSNVSQPYFGGDIGLIR	578.3402 636.3695 997.5207	583.3444 641.3737 1002.525
Ferritin (1188)	SQSNDLQALDAPR, FANGDPTALLVIDNELR	707.8497 929.4889	712.8538 934.493
Flavodoxin (1628)	DLLPGTETK, VPTDGYTFAESK	487.2637 657.8143	491.2708 661.8213
Ferredoxin (2042)	SGAVEQPDAMGVK, ADGFTLLCVAFPCSDLR	644.8137 971.4635	648.8208 976.4676

Table S5: global proteome data (see excel spreadsheet uploaded separately).